Journal of Computational Physics **168,** 412–432 (2001)
doi:10.1006/jcph.2001.6707, available online at http://www.idealibrary.com on IDEAL®

# A Fast Method for Solving Acoustic Scattering Problems in Frequency Bands

Rabia Djellouli, Charbel Farhat, and Radek Tezaur

*Department of Aerospace Engineering Sciences and Center for Aerospace Structures, University of Colorado at Boulder, Boulder, Colorado 80309-0429*
E-mail: Rabia.Djellouli@colorado.edu

Received February 21, 2000; revised November 30, 2000

We present a methodology for computing efficiently scattered fields in a frequency band. The main feature of this methodology is the construction of a series of discrete problems that differ only by their right-hand sides, rather than by both their left- and right-hand sides. Its key steps are (a) the reformulation of the acoustic scattering problem in a bounded domain using any preferred absorbing boundary condition, (b) the characterization of the repeated derivatives with respect to the frequency of the scattered field as solutions of scattering-type problems with different source terms and boundary conditions, and (c) the reconstruction of a scattered field by either the Padé approximants or Wynn's algorithm. We report on several multifrequency acoustic scattering examples that illustrate the accuracy and computational efficiency of the proposed solution methodology. 

*Key Words:* Helmholtz; guided waves; acoustic scattering; absorbing boundary condition; multiple frequencies; Padé approximants; Wynn's algorithm.

## 1. INTRODUCTION

The straightforward solution of acoustic scattering problems [1] with multiple frequencies leads to the solution of a set of linear systems of equations with different *left-* and right-hand sides, regardless of the method chosen for discretizing the governing exterior Helmholtz problem [2–5]. At relatively high frequencies, each of these systems of equations can be sufficiently large to overwhelm some of the largest computing resources that are currently available. The solution of such multiple systems of equations by a direct method requires the factorization of a number of matrices equal to the number of specified frequencies, and therefore leaves little room for reducing the CPU time. On the other hand, a few techniques have been developed for maximizing the computational efficiency of iterative schemes applied to the solution of a set of *near-by* problems (for example, see [6, 7]), but few if any significant successes have been published in the literature for the particular case of the



0021-9991/01 $35.00

Helmholtz problem. For this reason, we present in this paper an alternative approach for solving efficiently multifrequency acoustic scattering problems.

Our main idea is to construct a solution methodology that leads to the solution of a system of equations with multiple *right*-hand sides, rather than multiple systems of equations that differ by both their left- and right-hand sides. Indeed, the solution by a direct method of a system of equations with multiple right-hand sides is computationally efficient: the matrix of the system needs be factored only once, and the sought-after solutions are obtained by relatively inexpensive forward and backward substitutions. Furthermore, several iterative algorithms such as block GMRES [8], block QMR [9], and FETI-H [10, 11] have already been tuned for the solution of systems equations with multiple right-hand sides, and have demonstrated computational efficiency in the context of Helmholtz problems.

The key step of our methodology is the characterization of the first and higher derivatives of the scattered field with respect to the frequency as the solutions of a Helmholtz problem with different source terms and boundary conditions. However, the fact that we can establish this characterization only when the target acoustic scattering problem is formulated in a bounded domain using any absorbing boundary condition [12–16] sets the scope of this paper to such discretization methods of the exterior Helmholtz problem.

For the sake of clarity, we describe our solution methodology first in the context of guided wave problems. Then, we extend it to acoustic scattering problems. In both cases, we illustrate this methodology with several two-dimensional numerical examples that highlight its potential for reducing significantly the CPU time associated with the solution of multifrequency time-harmonic wave problems.

## 2. NOMENCLATURE AND ASSUMPTIONS

Throughout this paper, we adopt the following nomenclature and assumptions

- $\Omega$ is a bounded domain of $\mathbb{R}^d (d = 2, 3)$ representing an impenetrable obstacle.
- $\Omega^e = \mathbb{R}^d \backslash \bar{\Omega}$ is the homogeneous isotropic medium in $\mathbb{R}^d$ where the obstacle is embedded.
- $\Omega_b^e$ denotes the computational domain.
- $\Gamma$ is the boundary of $\Omega^e$ and is assumed to be Lipschitzian.
- $\Sigma$ is the fictitious boundary, that is, the boundary of $\Omega_b^e$; it is assumed to be Lipschitzian.
- $s$ is the curvilinear abscissa.
- $\zeta$ is the curvature (in two dimensions) of the artificial boundary $\Sigma$.
- $x$ is a point of $\mathbb{R}^d$, and $r = \|x\|_2$ is the distance from the origin point to $x$.
- $S^1 = \{x \in \mathbb{R}^d / \|x\|_2 = 1\}$ is the unit sphere in $\mathbb{R}^d$.
- $\nabla$ is the gradient operator in $\mathbb{R}^d$.
- $\Delta$ is the Laplacian operator in $\mathbb{R}^d$.
- $\nu$ is the outward normal to $\Gamma$, and $\frac{\partial}{\partial \nu}$ is the normal derivative operator.
- $k$ is a positive number representing the wavenumber of the incident wave.
- $\lambda = \frac{2\pi}{k}$ is a positive number representing the wavelength.
- $u(k) = u(k; x)$ for $x \in \mathbb{R}^d$.
- $d$ is a vector of the unit sphere $S^1$ representing the direction of the incident plane wave.
- $u^{(n)}(k)$ is the $n$-th derivative of $u(k)$ with respect to $k$, i.e., $u^{(n)}(k) = \frac{\partial^n u(k)}{\partial k^n}$.
- $L^2$ and $H^1$ are the standard Sobolev spaces [17].

• $H^1_{loc}(\Omega^e)$ is the space of functions that belong to $H^1(D)$ for any open-bounded set $D$ in $\Omega^e$ [17].

## 3. THE WAVEGUIDE MODEL PROBLEM

### 3.1. *Mathematical Formulation*

In this section, we consider the waveguide model problem graphically depicted in Fig. 1, and mathematically formulated as

$$\text{Find } u(k) \in H^1(\Omega) \text{ such that}$$

$$\begin{aligned} \Delta u(k) + k^2 u(k) &= 0 \quad \text{in } \Omega \\ u(k) &= 1 \quad \text{on } \Gamma_1 \\ \frac{\partial u(k)}{\partial \nu} &= 0 \quad \text{on } \Gamma_3 \cup \Gamma_4 \\ \frac{\partial u(k)}{\partial \nu} - iku(k) &= 0 \quad \text{on } \Gamma_2, \end{aligned} \tag{1}$$

where $\Gamma = \bigcup_{j=1}^{4} \Gamma_j$ is the boundary of the waveguide, and $i$ is the pure imaginary number satisfying $i^2 = -1$.

The exact solution of the boundary value problem (BVP) (1) is

$$u_{ex}(k) = e^{ikx_1} \quad \text{in } \Omega. \tag{2}$$

Hence, $u_{ex}(k)$ is an analytic function of $k \in \mathbb{R}$ whose Taylor's expansion with respect to $k$ can be written as

$$u(k) = \sum_{n=0}^{\infty} \frac{(k-k_0)^n}{n!} u^{(n)}(k_0).$$

Next, we characterize the derivatives $(u^{(n)}(k))_{n\in\mathbb{N}}$.

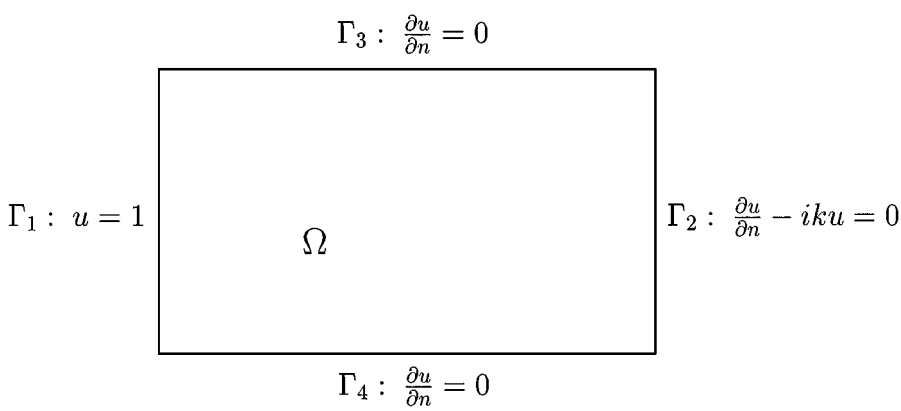


**FIG. 1.** A waveguide model problem.

3.2. *Characterization of the Derivatives $u^{(n)}(k)$*

Let

$$\begin{aligned} v_n(k) &= \frac{u^{(n)}(k)}{n!} \quad n \in \mathbb{N}^* \\ v_0(k) &= u(k) \\ v_{-1}(k) &= 0. \end{aligned} \tag{3}$$

From the differentiation of the BVP(1) with respect to $k$, it follows that for $n \geq 1$

$$\begin{aligned} \Delta v_n(k) + k^2 v_n(k) &= -2k v_{n-1}(k) - v_{n-2}(k) && \text{in } \Omega \\ v_n(k) &= 0 && \text{on } \Gamma_1 \\ \frac{\partial v_n(k)}{\partial \nu} &= 0 && \text{on } \Gamma_3 \cup \Gamma_4 \\ \frac{\partial v_n(k)}{\partial \nu} - ik v_n(k) &= i v_{n-1}(k) && \text{on } \Gamma_2, \end{aligned} \tag{4}$$

which shows that the members of the sequence $(v_n(k))_{n\in\mathbb{N}^*}$ are the solutions of BVPs that differ only by their source terms and one of the boundary conditions, that is, by their right-hand sides after discretization. This characterization suggests that, in principle, the following method for computing $u(k)$ for different values of $k \in \mathbb{R}$ is an efficient one:

Step 1. Compute the sequence $(v_n(k_0))_{n\in\mathbb{N}}$ for a focal wavenumber $k_0$.

Step 2. For each wavenumber of interest $k \neq k_0$, deduce $u(k)$ from Taylor's expansion

$$u(k) = \sum_{n=0}^{\infty} (\Delta k)^n v_n(k_0) \tag{5}$$

where

$$\Delta k = k - k_0.$$

In practice, the Taylor expansion (5) must be truncated, which raises the issue of the interval of convergence of the *numerical* algorithm chosen for evaluating this sum.

The two-step solution method summarized above is, in principle, computationally efficient because, once the BVP (1) is discretized—for example, by a finite element method—each discrete solution vector $\mathbf{v}_n(k_0)$ corresponding to $v_n(k_0)$ is obtained by solving

$$\left(\mathbf{K} - k_0^2 \mathbf{M} - ik_0 \mathbf{S}\right) \mathbf{v}_n(k_0) = \mathbf{f}_n \quad n \in \mathbb{N}, \tag{6}$$

where $\mathbf{K}$ and $\mathbf{M}$ are the standard stiffness and mass matrices, respectively, and $\mathbf{S}$ is the mass-like matrix associated with the discretization of the boundary condition specified on $\Gamma_2$. The vector $\mathbf{f}_0$ is dictated by the Dirichlet boundary condition of the BVP (1), and all subsequent $\mathbf{f}_n$ vectors are given by

$$\mathbf{f}_n = 2k_0 \mathbf{M} \mathbf{v}_{n-1}(k_0) + \mathbf{M} \mathbf{v}_{n-2}(k_0) + i \mathbf{S} \mathbf{v}_{n-1}(k_0) \quad n \geq 1. \tag{7}$$

Hence, the sequence of vectors $\mathbf{v}_n(k_0)$ is the solution of a system of equations with multiple right-hand sides. As stated earlier, such a system of equations can be solved efficiently by

either direct or iterative methods. As for the expansion (5), we report next on its evaluation by the Padé approximants [18], and Wynn's algorithm which is also known as the $\epsilon$-algorithm [19, 20].

### 3.3. *Numerical Examples*

Here, we consider a configuration of the waveguide shown in Fig. 1, where $\Omega$ is an $a \times a$ squared domain. We focus on three frequency bands $\mathcal{B}(k_0 a)$ centered around three different frequencies corresponding to $k_0 a = 6$, $k_0 a = 10$, and $k_0 a = 24$. For each frequency band, we discretize the computational domain by $a/h_{k_0} \times a/h_{k_0}$ Q1 finite elements, where $h_{k_0}$ is determined so that all the frequencies in $\mathcal{B}(k_0 a)$ are well resolved by the $a/h_{k_0} \times a/h_{k_0}$ mesh.

For each focal wavenumber $k_0$, we first solve Eqs. (6) and (7) to determine a certain sequence of vectors $\mathbf{v}_n(k_0)$. Then, we construct for various values of $k = k_0 + \Delta k$, $ka \in \mathcal{B}(k_0 a)$, the solutions $\mathbf{u}(k)$ by applying to Eq. (5) a Padé approximant $[L, M]$ ($L + M + 1$ terms; see Appendix A) and Wynn's approximation $(\mathcal{E}_p^n)$ of order $(n, p)$ (vector version, $n + p + 1$ terms; see Appendix B). In order to justify the usage of these two approximation methods, we also attempt to construct the solutions $\mathbf{u}(k)$ by computing directly $N$ terms of the Taylor series described in Eq. (5). We monitor the accuracy of all three approaches by computing for each of them and each wavenumber $k$ the relative error in $\Omega$ defined as follows

$$e(k) = \frac{\|u(k) - u_{ex}(k)\|_{L^2(\Omega)}}{\|u_{ex}(k)\|_{L^2(\Omega)}}. \tag{8}$$

Furthermore, for each wavenumber $k$ such that $ka \in \mathcal{B}(k_0 a)$, we also compute a finite element "reference" solution using the mesh associated with $\mathcal{B}(k_0 a)$; that is, we solve the system of equation

$$(\mathbf{K} - k^2 \mathbf{M} - ik\mathbf{S})\mathbf{u}(k) = \mathbf{f} \tag{9}$$

using the mesh associated with $\mathcal{B}(k_0 a)$. We report in Tables I–III the accuracy results obtained for the *best* Taylor, Padé, and Wynn approximations, and compare them with those of the reference solutions. We use the acronym DIV to indicate that a specific approximation method diverges for the desired $\Delta k$.

The following observations are noteworthy:

- For all three values of the wavenumber $k_0$, the Padé approximants and Wynn's algorithm improve the interval of convergence of the Taylor series by a factor ranging between 3 and 4.
- The Padé approximants and Wynn's algorithm appear to possess similar intervals of convergence and deliver comparable accuracy.
- For $k_0 a = 6$, $k_0 a = 10$, and $k_0 a = 24$ the proposed methodology delivers either the same accuracy as the straightforward approach (reference solutions), or reproduces the exact solution with less than 2.5% relative error, in the frequency bands $\mathcal{B}(6) = [1, 14]$, $\mathcal{B}(10) = [2, 18]$, and $\mathcal{B}(24) = [17, 31]$, respectively.
- Twenty-three terms at most are needed for the Padé or Wynn approximations to reconstruct the solutions $u(k)$ in the relatively large frequency bands identified above. This means that the main computational cost associated with sweeping on the frequency in these bands is that associated with the solution of a system of equations with 23 right-hand sides. Given that such a system can be solved efficiently by either a direct or smart iterative algorithm, the results reported in Tables I–III illustrate the potential of the proposed methodology for solving efficiently multifrequency time-harmonic wave problems.

**TABLE I**
**Accuracy Results for a Waveguide Problem and a Square-Shaped Geometry—$k_0a = 6$; $h_{k_0} = a/50$**

| $\Delta ka$ | $\frac{\lambda}{h_{k_0}}$ | Taylor $N$ | Taylor $e(k)$ | Padé $[L, M]$ | Padé $e(k)$ | Wynn $(n, p)$ | Wynn $e(k)$ | Reference $e(k)$ |
|---|---|---|---|---|---|---|---|---|
| 0 | 52.3 | | | | | | | 0.0023 |
| −5 | 314.0 | DIV | DIV | [8, 8] | 0.0023 | (0, 16) | 0.0023 | 1.8e-05 |
| −4 | 157.0 | DIV | DIV | [5, 5] | 0.0020 | (0, 10) | 0.0010 | 0.0001 |
| −3 | 104.7 | 25 | 0.0025 | [5, 5] | 0.0018 | (0, 10) | 0.0017 | 0.0003 |
| 3 | 34.9 | 22 | 0.0059 | [6, 6] | 0.0079 | (0, 12) | 0.0079 | 0.0075 |
| 4 | 31.4 | DIV | DIV | [7, 7] | 0.0098 | (0, 12) | 0.0096 | 0.0090 |
| 5 | 28.5 | DIV | DIV | [7, 7] | 0.0143 | (0, 12) | 0.0124 | 0.0128 |
| 6 | 26.2 | DIV | DIV | [7, 7] | 0.0181 | (0, 14) | 0.0181 | 0.0176 |
| 7 | 24.7 | DIV | DIV | [11, 11] | 0.0227 | (0, 24) | 0.0209 | 0.0203 |
| 8 | 22.4 | DIV | DIV | [11, 11] | 0.0368 | (0, 26) | 0.0278 | 0.0258 |
| 9 | 20.9 | DIV | DIV | [14, 14] | 0.0755 | (0, 26) | 0.0356 | 0.0339 |
| 10 | 19.6 | DIV | DIV | [18, 18] | 0.1798 | (0, 32) | 0.0395 | 0.0384 |
| 11 | 18.5 | DIV | DIV | DIV | DIV | (0, 32) | 0.0421 | 0.0454 |
| 12 | 17.4 | DIV | DIV | DIV | DIV | (0, 38) | 0.0610 | 0.0577 |
| 13 | 16.5 | DIV | DIV | DIV | DIV | (0, 30) | 0.1545 | 0.0651 |

**TABLE II**
**Accuracy Results for a Waveguide Problem and a Square-Shaped Geometry—$k_0a = 10$; $h_{k_0} = a/100$**

| $\Delta ka$ | $\frac{\lambda}{h_{k_0}}$ | Taylor $N$ | Taylor $e(k)$ | Padé $[L, M]$ | Padé $e(k)$ | Wynn $(n, p)$ | Wynn $e(k)$ | Reference $e(k)$ |
|---|---|---|---|---|---|---|---|---|
| 0 | 62.8 | | | | | | | 0.0022 |
| −9 | 628.0 | DIV | DIV | [8, 8] | 0.0713 | (0, 16) | 0.1260 | 2.71e-06 |
| −8 | 314.0 | DIV | DIV | [8, 8] | 0.0231 | (0, 16) | 0.0415 | 3.08e-05 |
| −7 | 209.3 | DIV | DIV | [8, 8] | 0.0060 | (0, 16) | 0.0099 | 7.92e-05 |
| −6 | 157.0 | DIV | DIV | [8, 8] | 0.0019 | (0, 10) | 0.0023 | 0.0001 |
| −5 | 125.6 | DIV | DIV | [8, 8] | 0.0013 | (0, 16) | 0.0013 | 0.0003 |
| −4 | 104.7 | DIV | DIV | [8, 8] | 0.0012 | (0, 14) | 0.0012 | 0.0005 |
| −3 | 89.7 | 8 | 0.0827 | [5, 5] | 0.0010 | (0, 10) | 0.0018 | 0.0007 |
| 3 | 48.3 | 8 | 0.0084 | [6, 6] | 0.0051 | (0, 12) | 0.0051 | 0.0050 |
| 4 | 44.9 | DIV | DIV | [6, 6] | 0.0064 | (0, 12) | 0.0064 | 0.0065 |
| 5 | 41.9 | DIV | DIV | [6, 6] | 0.0069 | (0, 12) | 0.0099 | 0.0085 |
| 6 | 39.3 | DIV | DIV | [8, 8] | 0.0100 | (0, 16) | 0.0100 | 0.0096 |
| 7 | 36.9 | DIV | DIV | [8, 8] | 0.0124 | (0, 16) | 0.0144 | 0.0115 |
| 8 | 34.9 | DIV | DIV | [8, 8] | 0.0255 | (0, 16) | 0.0473 | 0.0146 |
| 9 | 33.1 | DIV | DIV | [8, 8] | 0.0878 | (0, 16) | 0.1511 | 0.0163 |
| 10 | 31.4 | DIV | DIV | [8, 8] | 0.2068 | (0, 16) | 0.3382 | 0.0186 |

**TABLE III**
**Accuracy Results for a Waveguide Problem and a Square-Shaped Geometry—$k_0a = 24$; $h_{k_0} = a/150$**

| $\Delta ka$ | $\frac{\lambda}{h_{k_0}}$ | Taylor $N$ | Taylor $e(k)$ | Padé $[L, M]$ | Padé $e(k)$ | Wynn $(n, p)$ | Wynn $e(k)$ | Reference $e(k)$ |
|---|---|---|---|---|---|---|---|---|
| 0 | 39.2 | | | | | | | 0.0151 |
| −9 | 62.8 | DIV | DIV | [9, 9] | 0.1131 | (0, 18) | 0.2012 | 0.0038 |
| −8 | 58.8 | DIV | DIV | [9, 9] | 0.0455 | (0, 18) | 0.0801 | 0.0042 |
| −7 | 55.4 | DIV | DIV | [9, 9] | 0.0157 | (0, 18) | 0.0242 | 0.0051 |
| −6 | 52.3 | DIV | DIV | [9, 9] | 0.0082 | (0, 18) | 0.0096 | 0.0065 |
| −5 | 49.6 | DIV | DIV | [9, 9] | 0.0076 | (0, 18) | 0.0078 | 0.0072 |
| −4 | 47.1 | DIV | DIV | [8, 8] | 0.0083 | (0, 18) | 0.0083 | 0.0083 |
| −3 | 44.9 | 6 | 0.0868 | [3, 3] | 0.0059 | (0, 6) | 0.0102 | 0.0102 |
| −2 | 42.8 | 7 | 0.0062 | [2, 2] | 0.0082 | (0, 4) | 0.0092 | 0.0114 |
| 2 | 36.2 | 6 | 0.0281 | [4, 4] | 0.0182 | (0, 8) | 0.0182 | 0.0182 |
| 3 | 34.9 | DIV | DIV | [4, 4] | 0.0209 | (0, 8) | 0.0209 | 0.0213 |
| 4 | 33.6 | DIV | DIV | [5, 5] | 0.0221 | (0, 14) | 0.0237 | 0.0238 |
| 5 | 32.5 | DIV | DIV | [7, 7] | 0.0250 | (0, 14) | 0.0244 | 0.0253 |
| 6 | 31.4 | DIV | DIV | [7, 7] | 0.0246 | (0, 14) | 0.0254 | 0.0289 |
| 7 | 30.4 | DIV | DIV | [7, 7] | 0.0285 | (0, 18) | 0.0367 | 0.0324 |
| 8 | 29.4 | DIV | DIV | [9, 9] | 0.0539 | (0, 18) | 0.1190 | 0.0342 |
| 9 | 28.5 | DIV | DIV | [9, 9] | 0.1470 | (0, 20) | 0.2751 | 0.0381 |

## 4. THE SCATTERING PROBLEM

### 4.1. *Mathematical Formulation in a Bounded Domain*

Next, we consider the $d$-dimensional ($d = 2, 3$) scattering of time-harmonic acoustic waves by an impenetrable obstacle embedded in a homogeneous medium. This problem is governed by the BVP [1]

$$\begin{aligned} &\text{Find } u(k) \in H^1_{loc}(\Omega^e) \text{ such that} \\ &\Delta u(k) - k^2 u(k) = 0 \qquad \text{in } \Omega^e \\ &Bu = f(k) \quad \text{on } \Gamma \\ &\lim_{r\to\infty} r^{\frac{d-1}{2}} \left( \frac{\partial u(k)}{\partial r} - iku(k) \right) = 0, \end{aligned} \tag{10}$$

where

$$f(k) = -Be^{ikx.d}, \tag{11}$$

and $B$ is a boundary operator that characterizes the type of the scatterer [1]. More specifically, $B$ is a Neumann derivative operator for a sound-hard scatterer, a Dirichlet operator for a sound-soft scatterer, and an impedance operator for a scatterer with a lossy boundary. For simplicity but without any loss of generality, in this paper we consider the case of a sound-hard scatterer.

As stated in the introduction, for a scattering problem, we can establish a characterization of the derivatives $u^{(n)}(k)$ that is similar to that presented in Section 3.2, only when the BVP

(10) is first reformulated in a bounded domain. Such a step is also required when the exterior Helmholtz problem (10) is to be discretized by a domain-based method such as the finite difference or finite element method. The definition of a bounded computational domain is typically achieved by surrounding the scatterer by an artificial boundary positioned at a certain distance from the surface of the scatterer. The "far-field" behavior of the scattered field is then represented either by boundary conditions specified on the artificial boundary, or by assumed interpolation in the complement of the computational domain. In this work, we consider only the former approach, and more specifically nonreflecting or absorbing boundary conditions [12–16]. Using such an approach, we reformulate the BVP (10) as

$$\begin{aligned} &\text{Find } u(k) \in H^1\left(\Omega_b^e\right) \text{ such that} \\ &-\Delta u(k) - k^2 u(k) = 0 \qquad \text{in } \Omega_b^e \\ &\frac{\partial u(k)}{\partial \nu} = f(k) \quad \text{on } \Gamma \\ &\frac{\partial u(k)}{\partial \nu} - M(k)u(k) = 0 \qquad \text{on } \Sigma, \end{aligned} \tag{12}$$

where $M(k)$ is a differential operator, and the third of Eqs. (12) is a general representation of absorbing boundary conditions. Different approaches for constructing an absorbing boundary condition are usually associated with different approaches for approximating the Dirichlet-to-Neumann (DtN) operator [21, 27], and result in different expressions for $M(k)$. All absorbing boundary conditions share however the same objective, which is to reduce as much as possible the reflection of waves from the artificial boundary so that the resulting BVP (12) is well posed, and its solution is a "good" approximation of the restriction of the solution of the BVP (10) to $\Omega_b^e$.

The variational formulation of the BVP (12) goes as

$$\begin{aligned} &\text{Find } u(k) \in H^1\left(\Omega_b^e\right) \text{ such that} \\ &\mathcal{H}(u(k), v) = \mathcal{R}(v) \quad \forall v \in H^1\left(\Omega_b^e\right), \end{aligned} \tag{13}$$

where $\mathcal{H}(.,.)$ is a symmetric bilinear form defined on $H^1(\Omega_b^e) \times H^1(\Omega_b^e)$ by

$$\mathcal{H}(u, v) = \int_{\Omega_b^e} \nabla u \cdot \nabla v \, dx - k^2 \int_{\Omega_b^e} uv \, dx - \int_{\Sigma} M(k) uv \, ds \tag{14}$$

and $\mathcal{R}(\cdot)$ is a linear form defined on $L^2(\Omega_b^e)$ by

$$\mathcal{R}(v) = \int_{\Gamma} f(k) v \, dx. \tag{15}$$

### 4.2. *Characterization of the Derivatives of the Scattered Field with Respect to k*

It is well known (for example, see [22] and the references therein) that the solution $u(k)$ of the BVP (10) is a meromorphic function of $k \in \mathbb{C}$, with poles in the half-plane $\Im(k) < 0$. Consequently, $u(k)$ can be expanded as a Taylor series with respect to $k$ in the interval $]0, \infty[$. However, it does not seem possible to derive for the BVP (10) a characterization of the derivatives $u^n(k)$ that is similar to the one described in Section 3.2. On the other

hand, for all classical local absorbing conditions, the function $k \to M(k)$ is analytic in the interval $]0, \infty[$, which implies that the solution $u(k)$ of the BVP (12) can also be expanded as a Taylor series with respect to $k$. Furthermore, it turns out that for the BVP (12), we are able to characterize the derivatives of $u(k)$ with respect to $k$ as in Section 3.2, and therefore to exploit the expansion of $u(k)$ with respect to $k$.

For this purpose, we reintroduce the sequence $(v_n(k))_{n\in\mathbb{N}}$ defined in Eqs. (3) and differentiate the BVP (12) with respect to $k$. This leads to

$$\begin{aligned} -\Delta v_n(k) - k^2 v_n(k) &= 2k v_{n-1}(k) + v_{n-2}(k) && \text{in } \Omega \\ \frac{\partial v_n(k)}{\partial \nu} &= \frac{1}{n!} f^{(n)}(k) && \text{on } \Gamma \\ \frac{\partial v_n(k)}{\partial \nu} - M(k) v_n(k) &= \sum_{p=1}^{n} \frac{1}{p!} M^{(p)}(k) v_{n-p}(k) && \text{on } \Sigma, \end{aligned} \tag{16}$$

which shows that every $v_n(k)$ is the solution of the variational problem

$$\mathcal{H}(v_n(k), v) = \mathcal{R}_n(v) \quad \forall v \in H^1\big(\Omega_b^e\big), \tag{17}$$

where $\mathcal{R}_n(\cdot)$ is a linear form defined on $L^2(\Omega_b^e)$ by

$$\begin{aligned} \mathcal{R}_0(v) &= \int_\Gamma f(k) v \, dx \\ \mathcal{R}_n(v) &= \int_\Gamma \frac{1}{n!} f^{(n)}(k) v \, dx + 2k \int_{\Omega_b^e} v_{n-1}(k) v \, dx \\ &\quad + \int_{\Omega_b^e} v_{n-2}(k) v \, dx + \sum_{p=1}^{n} \frac{1}{p!} \int_\Sigma M^{(p)}(k) v_{n-p}(k) v \, ds \quad n \geq 1. \end{aligned} \tag{18}$$

From Eqs. (14, 17, 18), it follows that $(v_n(k))_{n\in\mathbb{N}^*}$ are the solutions of BVPs that differ only by their source terms and their boundary conditions, that is, by their right-hand sides after discretization. This characterization of the derivatives $u^{(n)}(k)$ explains why, in principle, the methodology outlined in Section 3.2 is also attractive for solving multifrequency acoustic scattering problems.

### 4.3. *A Bayliss–Turkel-like Absorbing Boundary Condition*

In all examples discussed in the remainder of this paper, we adopt the second-order Bayliss–Turkel-like boundary condition originally developed in [21] for on-the-surface applications, and recently extended in [23] for finite element applications. However, we remind the reader that the solution method we propose in this paper works with any non-reflecting boundary condition of the form $\frac{\partial u(k)}{\partial \nu} - M(k)u(k) = 0$, including, for example, Keller and Givoli's DtN condition [27].

In two dimensions, the differential operator $M(k)$ associated with the Bayliss–Turkel-like absorbing boundary condition is

$$M(k)v = \left(ik - \frac{\zeta}{2}\right) v + \frac{\zeta^2}{8(\zeta - ik)} v + \frac{\partial}{\partial s}\left(\frac{1}{2(\zeta - ik)} \frac{\partial v}{\partial s}\right), \tag{19}$$

where $s$ and $\zeta$ are the curvilinear abscissae and the curvature on the fictitious boundary $\Sigma$, respectively. From Eq. (19), it follows that

$$\int_\Sigma M(k)uv\,ds = ik\int_\Sigma u\cdot v\,ds - \frac{1}{2}\int_\Sigma \zeta uv\,ds + \frac{1}{8}\int_\Sigma \frac{\zeta^2}{(\zeta - ik)}uv\,ds - \frac{1}{2}\int_\Sigma \frac{1}{(\zeta - ik)}\frac{\partial u}{\partial s}\frac{\partial v}{\partial s}\,ds. \tag{20}$$

For the differential operator $M(k)$ specified in (19), the sequence of derivatives $(M^{(p)}(k))_{p\in\mathbb{N}^*}$ satisfies

$$\int_\Sigma M^{(1)}(k)uv\,ds = i\int_\Sigma uv\,ds + \frac{1}{8}\int_\Sigma \zeta^2\frac{i}{(\zeta - ik)^2}uv\,ds - \frac{1}{2}\int_\Sigma \frac{i}{(\zeta - ik)^2}\frac{\partial u}{\partial s}\frac{\partial v}{\partial s}\,ds \tag{21}$$

$$\int_\Sigma M^{(p)}(k)uv\,ds = \frac{1}{8}\int_\Sigma \zeta^2\frac{p!i^p}{(\zeta - ik)^{p+1}}uv\,ds - \frac{1}{2}\int_\Sigma \frac{p!i^p}{(\zeta - ik)^{p+1}}\frac{\partial u}{\partial s}\frac{\partial v}{\partial s}ds \quad p\geq 2.$$

Hence, the sequence of derivatives $(M^{(p)}(k))_{p\in\mathbb{N}^*}$ generated by the characterization (16) of the derivatives $u^{(n)}(k)$ incurs simply the construction of basic mass and stiffness matrices on the fictitious boundary $\Sigma$.

### 4.4. *Applications*

Here, our objective is to highlight the potential of the proposed methodology for solving efficiently multifrequency acoustic scattering problems. For this purpose, we consider two different two-dimensional problems involving two different scatterers but the same direction

$$d = \begin{bmatrix} \frac{\sqrt{2}}{2} \\ \frac{\sqrt{2}}{2} \end{bmatrix}$$

of the incident plane wave (see Eq. (11)). In the first problem, the scatterer is a disk of radius $a$. In the second one, it is a submarine-shaped flat object of length $2a$ (Fig. 2). For both problems, we design the exterior artificial boundary $\Sigma$ as a circle of radius $R = a + m\lambda$, where $m$ is a positive number. For each problem, we consider a sequence of frequency bands $\mathcal{B}(k_0a)$ associated with a sequence of increasing focal frequencies whose corresponding wavenumbers are denoted by $k_0$. For each frequency band, we apply the solution methodology proposed in this paper to compute the scattered fields $u(k)$, $k = k_0 + \Delta k$. Given the results obtained for the waveguide problem discussed in Section 3.3, we use a [10, 10] Padé approximant and a (0, 20) or (0, 28) Wynn approximation (scalar version; see Appendix B) to reconstruct the solution vectors $\mathbf{u}(k_0 + \Delta k)$.

In all cases, we discretize the computational domain by P1 finite elements, and unless otherwise specified, solve the resulting algebraic systems of equations by the FETI-H iterative method [10] equipped with the multiple right-hand side accelerator described in [11].

As in Section 3.3, for each wavenumber $k$ such that $ka \in \mathcal{B}(k_0a)$, we also compute a finite element reference solution using the mesh associated with $\mathcal{B}(k_0a)$. We assess the accuracy

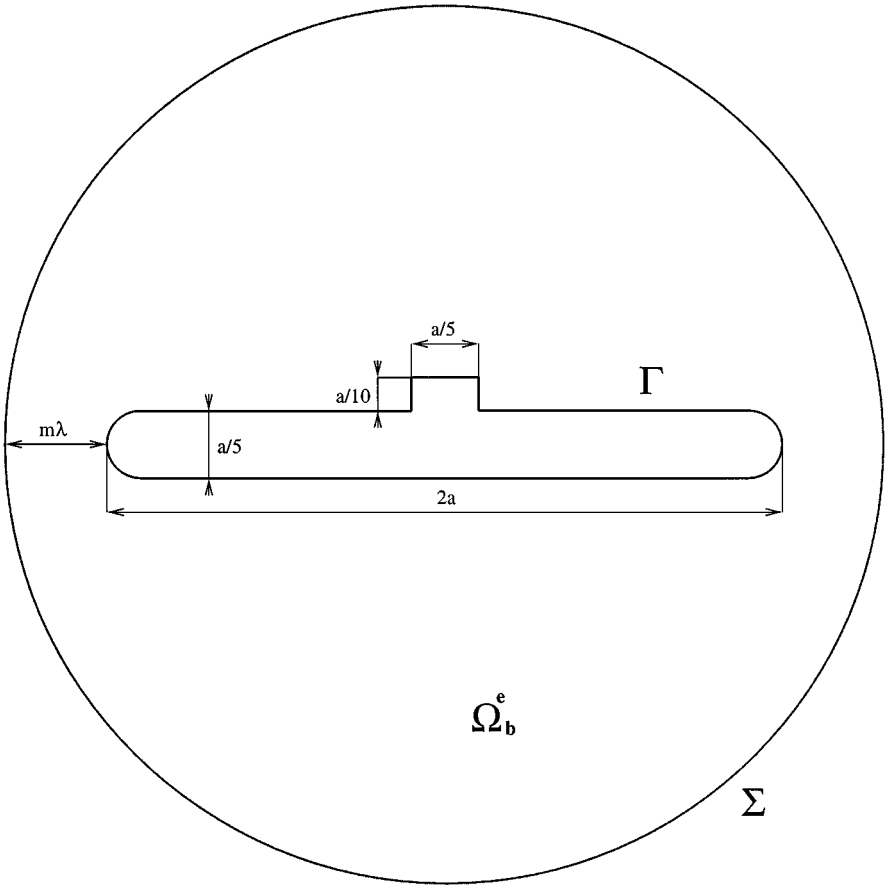


**FIG. 2.** A submarine-shaped scatterer: the computational domain.

of the reference solutions and that of the solutions reconstructed by the Taylor, Padé, and Wynn approximations by evaluating for each one of them a relative error computed as in Eq. (8), but where the $L_2$-norm on $\Omega$ is replaced by the $L_2$-norm on the surface of the scatterer $\Gamma$.

We perform all computations in double arithmetic precision on a Silicon Graphics Origin 2000 system.

*4.4.1. Scattering of time-harmonic waves by a disk.* For this problem, an analytical form of the exact solution can be found in [1]. We consider three different focal frequencies corresponding to $k_0a = 1$, $k_0a = 5$; and $k_0a = 31$. For $k_0a = 1$, we set the artificial boundary $\Sigma$ at $0.25\lambda$ from the surface of the scatterer ($m = 0.25$) and discretize the computational domain into $N_{\text{mesh}} = 1,424$ grid points. For $k_0a = 5$, we set $\Sigma$ at $m = 1.27\lambda$ and generate a mesh with $N_{\text{mesh}} = 34,931$ grid points. For $k_0a = 31$, we set $m = 8\lambda$ and generate a fine mesh with 1, 297, 196 grid points. We note that these meshes have been tailored to deliver a comparable accuracy for all three focal frequencies considered here. Indeed, using for each focal frequency its assigned mesh, we obtain three reference solutions for the three different scattering problems, which exhibit similar relative errors of the order of $10^{-3}$.

**TABLE IV**
**The Disk Scattering Problem: Accuracy Results — $k_0a = 1$; $h_{k_0} = a/6.3$; $m = 0.25$; $N_{\text{mesh}} = 1{,}424$**

| $\Delta ka$ | $\frac{\lambda}{h_{k_0}}$ | Taylor 20 $\epsilon(k)$ | Padé [10, 10] $\epsilon(k)$ | Wynn (0, 20) $\epsilon(k)$ | Reference $\epsilon(k)$ |
|---|---|---|---|---|---|
| 0 | 40.0 | | | | 0.0053 |
| −0.9 | 400.0 | DIV | 0.0369 | 0.0258 | 0.0255 |
| −0.75 | 160.0 | DIV | 0.0171 | 0.0169 | 0.0169 |
| −0.5 | 80.0 | 0.0093 | 0.0092 | 0.0092 | 0.0092 |
| −0.25 | 53.3 | 0.0036 | 0.0036 | 0.0036 | 0.0036 |
| 0.25 | 32.0 | 0.0080 | 0.0080 | 0.0080 | 0.0080 |
| 0.5 | 26.7 | 0.0092 | 0.0092 | 0.0092 | 0.0092 |
| 1.0 | 20.0 | DIV | 0.0107 | 0.0107 | 0.0107 |
| 1.5 | 16.0 | DIV | 0.0143 | 0.0143 | 0.0142 |
| 2.0 | 13.3 | DIV | 0.0359 | 0.0212 | 0.0194 |
| 2.5 | 11.4 | DIV | 0.1140 | 0.0446 | 0.0252 |

We report in Tables IV–VI the relative errors obtained for the 20-term Taylor series, the [10, 10] Padé approximant, the Wynn approximation of order (0, 20), and the reference solutions. These results show that

- depending on the wavenumber $k_0$, the Padé approximant and Wynn's algorithm improve the interval of convergence of the Taylor series by a factor ranging between 3 and 4.
- the Padé approximant and Wynn's algorithm have similar intervals of convergence and deliver comparable accuracy.

**TABLE V**
**The Disk Scattering Problem: Accuracy Results—$k_0a = 5$; $h_{k_0} = a/31.8$; $m = 1.27$; $N_{\text{mesh}} = 34{,}931$**

| $\Delta ka$ | $\frac{\lambda}{h_{k_0}}$ | Taylor 20 $\epsilon(k)$ | Padé [10,10] $\epsilon(k)$ | Wynn (0,20) $\epsilon(k)$ | Reference $\epsilon(k)$ |
|---|---|---|---|---|---|
| 0 | 40.0 | | | | 0.0017 |
| −3.0 | 100.0 | DIV | 0.1421 | 0.1844 | 0.0011 |
| −2.5 | 80.0 | DIV | 0.0197 | 0.0169 | 0.0010 |
| −2.0 | 66.7 | DIV | 0.0021 | 0.0019 | 0.0015 |
| −1.5 | 57.1 | DIV | 0.0022 | 0.0022 | 0.0022 |
| −1.0 | 50.0 | 0.0869 | 0.0021 | 0.0021 | 0.0021 |
| −0.5 | 44.4 | 0.0016 | 0.0016 | 0.0016 | 0.0016 |
| 0.5 | 36.4 | 0.0028 | 0.0028 | 0.0028 | 0.0028 |
| 1.0 | 33.4 | 0.0891 | 0.0036 | 0.0036 | 0.0036 |
| 1.5 | 30.8 | DIV | 0.0039 | 0.0039 | 0.0039 |
| 2.0 | 28.6 | DIV | 0.0043 | 0.0043 | 0.0037 |
| 2.5 | 26.7 | DIV | 0.0086 | 0.0083 | 0.0039 |
| 3.0 | 25.0 | DIV | 0.0310 | 0.0283 | 0.0050 |
| 3.5 | 23.5 | DIV | 0.0785 | 0.0697 | 0.0063 |

**TABLE VI**
**The Disk Scattering Problem: Accuracy Results—$k_0a = 31$; $h_{k_0} = a/200$; $m = 8$; $N_{\text{mesh}} = 1{,}297{,}196$**

| $\Delta ka$ | $\frac{\lambda}{h_{k_0}}$ | Taylor 20 $\epsilon(k)$ | Padé [10,10] $\epsilon(k)$ | Wynn (0,20) $\epsilon(k)$ | Reference $\epsilon(k)$ |
|---|---|---|---|---|---|
| 0 | 40 | | | | 0.0028 |
| −4.0 | 45.8 | DIV | 0.0980 | 0.0980 | 0.0022 |
| −3.5 | 45.0 | DIV | 0.0278 | 0.0249 | 0.0022 |
| −3.0 | 44.2 | DIV | 0.0081 | 0.0081 | 0.0023 |
| −2.0 | 42.7 | DIV | 0.0026 | 0.0026 | 0.0026 |
| −1.0 | 41.3 | 0.0031 | 0.0026 | 0.0026 | 0.0026 |
| 1.0 | 38.7 | 0.0034 | 0.0031 | 0.0031 | 0.0031 |
| 2.0 | 37.6 | DIV | 0.0032 | 0.0032 | 0.0031 |
| 3.0 | 36.5 | DIV | 0.0118 | 0.0118 | 0.0035 |
| 3.5 | 35.9 | DIV | 0.0278 | 0.0278 | 0.0037 |
| 4.0 | 35.4 | DIV | 0.0732 | 0.0732 | 0.0036 |

• for $k_0a = 1$, $k_0a = 5$, and $k_0a = 31$ the proposed methodology delivers either the same accuracy as the straightforward approach (reference solutions), or reproduces the exact solution with less than 3% relative error, in the frequency bands $\mathcal{B}(1) = [0.1, 3]$, $\mathcal{B}(5) = [2.5, 8]$, and $\mathcal{B}(31) = [27.5, 34.5]$, respectively.

Besides the cost of solving one Helmholtz problem to compute $u(k_0)$, the main computational cost of the method proposed in this paper for solving multifrequency time-harmonic wave problems is by far that associated with the characterization of the derivatives $u^{(n)}(k)$. As established in Section 3.2 and Section 4.2, this characterization requires solving a system of equations with a number of right-hand sides equal to the number of terms that must be included in the Padé or Wynn algorithms to achieve the desired level of accuracy. Experience reveals that using a number of terms in the neighborhood of 20 delivers an excellent accuracy (see Tables I–VI). After this system of equations is solved, the scattered field can be reconstructed at relatively no computational cost, for any frequency $k = k_0 + \Delta k$, where $|\Delta k|$ is in the convergence interval of the Padé or Wynn algorithms. It follows that if the system of equations associated with the characterization of the derivatives $u^{(n)}(k)$ is solved by a direct method, the proposed computational methodology can be expected to be feasible even for a two-frequency problem, and can also be expected to speed up the solution time of the straightforward approach (multiple left-hand side problems) by a factor almost as large as the number of successfully sampled frequencies. However, if the system of equations associated with the characterization of $u^{(n)}(k)$ is solved by an iterative method tuned for the solution of systems with multiple right-hand sides, the proposed computational methodology could be feasible only if the number of successfully sampled frequencies is larger than a certain threshold that depends on the chosen iterative solver. This is illustrated in Table VII for the scattering problem considered here, where 21 terms are included in either the Padé or Wynn approximations, and where the system of equations associated with the characterization of the derivatives is solved by the accelerated FETI-H method [10, 11]. The performance results reported in Table VII show that in this case, our computational methodology is feasible when the scattered field is to be computed

**TABLE VII**
**The Disk Scattering Problem: CPU Performance Results on an Origin 2000 System 21-Term of a Padé of Wynn Approximation—FETI-H Iterative Solver**

| | $k_0a = 5$<br>$\mathcal{B}(5) = [2.5, 8.0]$<br>$N_{\text{mesh}} = 34,931$<br>10 processors | $k_0a = 31$<br>$\mathcal{B}(31) = [27.5, 34.5]$<br>$N_{\text{mesh}} = 1,297,196$<br>20 processors |
|---|---|---|
| CPU time for 1 frequency | 5 seconds | 304 seconds |
| CPU time for more than 2 frequencies | 18 seconds | 1,742 seconds |
| Breaking point | 4 frequencies | 6 frequencies |
| Speedup factor for a sweep by increments of $\Delta ka = 0.5$ | 3.3 | 2.8 |

for at least four different frequencies when $k_0a = 5$, and six different frequencies when $k_0a = 31$. The speedup factor it delivers depends, among others, on the size of the increment used in the frequency sweep. For example, for a sweep by increments of $\Delta ka = 0.5$, the width of the frequency band for which the Padé [10, 10] and Wynn (0, 20) approximations achieve an excellent accuracy is such that for $k_0a = 5$, our computational methodology achieves a speedup factor equal to 3.3, and for $k_0a = 31$, it achieves a speedup factor equal to 2.8.

*4.4.2. Scattering of time-harmonic waves by a submarine-shaped flat obstacle.* For this problem, which is graphically depicted in Fig. 2, the exact solution is not available. Consequently, we assess the accuracy of the Taylor, Padé, and Wynn approximations by comparing the solutions they generate with those of the straightforward approach (multiple left-hand sides), that is, with the reference solutions. Hence, for this problem, we define the relative error as

$$\tilde{\epsilon}(k) = \frac{\|u(k) - \tilde{u}(k)\|_{L^2(\Gamma)}}{\|\tilde{u}(k)\|_{L^2(\Gamma)}}, \tag{22}$$

where the tilde notation is used to designate the reference solution.

As for the previous scattering problem, we consider several focal frequencies corresponding to $k_0a = 2$, $k_0a = 8$, $k_0a = 31$, and $k_0a = 63$. In each case, we set the artificial boundary at $a + \lambda$ from the center of the scatterer ($m = 1$), and generate an unstructured mesh using 40 elements per focal wavelength as a guideline ($\lambda / h_{k_0} \approx 40$).

For each sampled frequency in the neighborhood of one of the four focal frequencies, we compute a reference solution, and reconstruct three other solutions using a 20-term Taylor series, the [10, 10] Padé approximant, and the Wynn approximation of order (0, 28). We report on the accuracy of the latter solutions in Tables VIII–XI. We note that

- as in the previous examples, depending on the wavenumber $k_0$, the Padé approximant and Wynn's algorithm improve the interval of convergence of the Taylor series by a factor ranging between 3 and 5,
- the Padé approximant and Wynn's algorithm exhibit similar intervals of convergence, but Wynn's algorithm reconstructs a slightly more accurate solution, and
- for $k_0a = 2$, $k_0a = 8$, $k_0a = 31$, and $k_0a = 63$ our methodology for performing efficiently a frequency sweep reproduces the reference solutions with less than 4% relative

**TABLE VIII**
**The Submarine Scattering Problem: Accuracy Results—$k_0a = 2.0$; $h_{k_0} = a/13$; $m = 1$; $N_{\text{mesh}} = 13{,}810$**

| $\Delta ka$ | $\frac{\lambda}{h_{k_0}}$ | Taylor 20 $\tilde{\epsilon}(k)$ | Padé [10, 10] $\tilde{\epsilon}(k)$ | Wynn (0, 28) $\tilde{\epsilon}(k)$ |
|---|---|---|---|---|
| 0 | 40 | | | |
| −1.75 | 320.00 | DIV | 0.0497 | 0.0288 |
| −1.5 | 160.00 | DIV | 0.0138 | 0.0023 |
| −1.0 | 80.00 | 0.5318 | 0.0000 | 0.0000 |
| −0.5 | 53.33 | 0.0000 | 0.0000 | 0.0000 |
| 0.5 | 32.00 | 0.0000 | 0.0000 | 0.0000 |
| 1.0 | 26.67 | 0.2364 | 0.0000 | 0.0000 |
| 1.5 | 22.86 | DIV | 0.0007 | 0.0000 |
| 2.0 | 20.00 | DIV | 0.0108 | 0.0056 |
| 2.5 | 17.78 | DIV | 0.0556 | 0.0329 |

error, in the frequency bands $\mathcal{B}(2) = [0.25, 4.5]$, $\mathcal{B}(8) = [4.5, 12]$, $\mathcal{B}(31) = [26, 36]$, and $\mathcal{B}(63) = [57.5, 68.5]$, respectively.

We also report in Table XII the CPU performance results obtained using the 29-term Wynn approximation for two different cases. In the first case, we solve the system of equations associated with the characterization of the derivatives by the accelerated FETI-H iterative algorithm [10, 11]. In the second case, we solve it by an optimized direct skyline method

**TABLE IX**
**The Submarine Scattering Problem: Accuracy Results—$k_0a = 8$; $h_{k_0} = a/50$; $m = 1$; $N_{\text{mesh}} = 44{,}090$**

| $\Delta ka$ | $\frac{\lambda}{h_{k_0}}$ | Tylor 20 $\tilde{\epsilon}(k)$ | Padé [10, 10] $\tilde{\epsilon}(k)$ | Wynn (0, 28) $\tilde{\epsilon}(k)$ |
|---|---|---|---|---|
| 0 | 40 | | | |
| −4.0 | 81.51 | DIV | 0.1181 | 0.0864 |
| −3.5 | 72.14 | DIV | 0.0417 | 0.0347 |
| −3.0 | 64.71 | DIV | 0.0109 | 0.0064 |
| −2.5 | 58.66 | DIV | 0.0016 | 0.0008 |
| −2.0 | 53.64 | DIV | 0.0000 | 0.0000 |
| −1.5 | 49.43 | DIV | 0.0000 | 0.0000 |
| −1.0 | 45.81 | 0.0037 | 0.0000 | 0.0000 |
| 1.0 | 34.46 | 0.0048 | 0.0000 | 0.0000 |
| 1.5 | 33.56 | DIV | 0.0000 | 0.0000 |
| 2.0 | 31.86 | DIV | 0.0000 | 0.0000 |
| 2.5 | 30.32 | DIV | 0.0007 | 0.0002 |
| 3.0 | 28.92 | DIV | 0.0054 | 0.0014 |
| 3.5 | 27.65 | DIV | 0.0214 | 0.0060 |
| 4.0 | 26.48 | DIV | 0.0434 | 0.0187 |
| 4.5 | 25.41 | DIV | 0.0818 | 0.0478 |

**TABLE X**

**The Submarine Scattering Problem: Accuracy**

**Results—$k_0a = 31$; $h_{k_0} = a/200$; $m = 1$; $N_{\text{mesh}} = 239{,}524$**

| $\Delta ka$ | $\frac{\lambda}{h_{k_0}}$ | Taylor $\tilde{\epsilon}(k)$ | Padé [10, 10] $\tilde{\epsilon}(k)$ | Wynn (0, 28) $\tilde{\epsilon}(k)$ |
|---|---|---|---|---|
| 0 | 40 | | | |
| −6.0 | 49.44 | DIV | 0.1391 | 0.1016 |
| −5.5 | 48.48 | DIV | 0.0758 | 0.0639 |
| −5.0 | 47.57 | DIV | 0.0423 | 0.0310 |
| −4.5 | 46.68 | DIV | 0.0198 | 0.0179 |
| −4.0 | 45.83 | DIV | 0.0078 | 0.0036 |
| −3.0 | 44.22 | DIV | 0.0004 | 0.0001 |
| −2.0 | 42.71 | DIV | 0.0000 | 0.0000 |
| −1.5 | 42.00 | 0.0022 | 0.0000 | 0.0000 |
| −1.0 | 41.31 | 0.0000 | 0.0000 | 0.0000 |
| 1.0 | 38.76 | 0.0000 | 0.0000 | 0.0000 |
| 1.5 | 38.17 | 0.0025 | 0.0000 | 0.0000 |
| 2.0 | 37.60 | DIV | 0.0000 | 0.0000 |
| 3.0 | 36.51 | DIV | 0.0002 | 0.0000 |
| 4.0 | 35.48 | DIV | 0.0055 | 0.0036 |
| 5.0 | 34.50 | DIV | 0.0383 | 0.0215 |
| 5.5 | 34.04 | DIV | 0.0719 | 0.0448 |
| 6.0 | 33.58 | DIV | 0.1182 | 0.0853 |

**TABLE XI**

**The Submarine Scattering Problem: Accuracy**

**Results—$k_0a = 63.0$; $h_{k_0} = a/400$; $m = 1$; $N_{\text{mesh}} = 973{,}288$**

| $\Delta ka$ | $\frac{\lambda}{h_{k_0}}$ | Taylor 20 $\tilde{\epsilon}(k)$ | Padé [10, 10] $\tilde{\epsilon}(k)$ | Wynn (0, 28) $\tilde{\epsilon}(k)$ |
|---|---|---|---|---|
| 0 | 40 | | | |
| −6.0 | 44.09 | DIV | 0.0972 | 0.0518 |
| −5.5 | 43.71 | DIV | 0.0560 | 0.0246 |
| −5.0 | 49.93 | DIV | 0.0295 | 0.0106 |
| −4.5 | 42.96 | DIV | 0.0142 | 0.0042 |
| −4.0 | 42.59 | DIV | 0.0054 | 0.0010 |
| −3.0 | 41.88 | DIV | 0.0002 | 0.0000 |
| −2.0 | 41.20 | 0.0962 | 0.0000 | 0.0000 |
| −1.0 | 40.53 | 0.0000 | 0.0000 | 0.0000 |
| 1.0 | 39.27 | 0.0000 | 0.0000 | 0.0000 |
| 2.0 | 38.66 | 1.027 | 0.0000 | 0.0000 |
| 3.0 | 38.08 | DIV | 0.0003 | 0.0000 |
| 4.0 | 37.51 | DIV | 0.0098 | 0.0014 |
| 4.5 | 37.23 | DIV | 0.0145 | 0.0048 |
| 5.0 | 36.96 | DIV | 0.0511 | 0.0159 |
| 5.5 | 36.70 | DIV | 0.0592 | 0.0397 |
| 6.0 | 36.42 | DIV | 0.1068 | 0.0687 |

**TABLE XII**
**The Submarine Scattering Problem CPU Performance Results on an Origin 2000 System**
**29-Term Wynn Approximation—FETI-H Solver vs Direct Skyline Solver**

| | $k_0a = 31$<br>$\mathcal{B}(31) = [26, 36]$<br>$N_{\text{mesh}} = 239,524$<br>10 processors | $k_0a = 63$<br>$\mathcal{B}(63) = [57.5, 68.5]$<br>$N_{\text{mesh}} = 973,288$<br>10 processors |
|---|---|---|
| CPU time | 59 seconds (FETI-H) | 405 seconds (FETI-H) |
| for 1 frequency | 235 seconds (direct) | 2,606 seconds (direct) |
| CPU time | 420 seconds (FETI-H) | 2,771 seconds (FETI-H) |
| for more than 2 frequencies | 558 seconds (direct) | 4,846 seconds (direct) |
| Breaking point | 7 frequencies (FETI-H) | 7 frequencies (FETI-H) |
| | 2 frequencies (direct) | 2 frequencies (direct) |
| Speedup factor for a sweep | 3.0 (FETI-H) | 3.5 (FETI-H) |
| by increments of $\Delta ka = 0.5$ | 9.2 (direct) | 12.9 (direct) |

[24] after we have renumbered the equations for optimal storage and arithmetic complexity by the Reverse Cuthill McKee algorithm [25]. Both the FETI-H and optimized direct skyline solvers are parallelized on the Origin 2000 system. The obtained CPU performance results show that for this scattering problem

- when the system of equations associated with the characterization of the derivatives is solved by the accelerated FETI-H iterative algorithm [10, 11], the proposed computational method is feasible when at least seven frequencies are sampled in either $\mathcal{B}(31)$ or $\mathcal{B}(63)$. On the other hand, when this system of equations is solved by an optimized direct skyline method, it is feasible as soon as two frequencies are sampled in either $\mathcal{B}(31)$ or $\mathcal{B}(63)$;
- for frequency sweeps by increments of $\Delta ka = 0.5$, our method equipped with the accelerated FETI-H solver [10, 11] achieves a speedup factor equal to 3.0 when sweeping in $\mathcal{B}(31)$, and a speedup factor equal to 3.5 when sweeping in $\mathcal{B}(63)$. When equipped with a direct skyline solver, these speedup factors increase to 9.2 and 12.9, respectively; and
- nevertheless, our computational method is several times faster when equipped with the FETI-H solver (and perhaps any other fast iterative solver) than with an optimized direct skyline solver.

## 5. THE PADÉ APPROXIMANTS VS WYNN'S ALGORITHM

Finally, we report in this section on our experience with the Padé and Wynn approximation methods. Computing a Padé approximant requires inverting for each point on $\Gamma$ an $M \times M$ matrix $\mathbf{C}$—in our case, typically a $10 \times 10$ matrix—after which the reconstruction of the sought-after solutions for all frequencies in the interval of convergence of this method incurs only evaluations of rational functions. For $M > 10$, $\mathbf{C}$ becomes so ill-conditioned that the evaluation of the Padé approximant becomes very difficult.

On the other hand, for each frequency in the interval of convergence, Wynn's algorithm requires recomputing the partial Taylor sums and reperforming the epsilon algorithm. Hence, when the number of target frequencies is large, Wynn's algorithm becomes more computationally expensive than Padé's method.

The scalar implementation of Wynn's approximation of order (0, 2L) is in theory equivalent to the $[L, L]$ Padé approximat. For $L \leq 10$, both approximations deliver comparable accuracy. For $L > 10$, often only Wynn's algorithm is sufficiently stable.

## 6. CONCLUSION

By characterizing the derivatives of the scattered field with respect to the frequency as the solutions of scattering-type problems with different source terms and boundary conditions, we have shown that multifrequency acoustic scattering problems can be solved at the computational cost of the solution of a single system of equations with multiple right-hand sides. The size of this system of equations is the same as that of the system of equations arising from the discretization of the exterior Helmholtz problem for any given frequency. The number of right-hand sides is equal to the number of terms required by a Padé- or Wynn-type algorithm for reconstructing accurately the scattered field for the wavenumber $k + \delta k$, knowing its value and the values of its derivatives for the wavenumber $k$. This characterization holds when the acoustic scattering problem is formulated in a bounded domain, using an absorbing boundary condition. It also holds when the artificial boundary is replaced by a finite thickness layer designed to damp all the waves entering it from the side of the scatterer, as in the perfectly matched layer technique of Berenger [26]. The results obtained for the solution via this characterization of various multifrequency guided wave and acoustic scattering problems for $1 \leq ka \leq 63$ suggest that the required number of Padé or Wynn terms is around 20. They also suggest that the interval of convergence of the proposed solution methodology is of the order of $ka \pm 5$. Sweeping on $ka$ in such intervals by increments $\Delta ka = 0.5$ typically results in a speedup factor equal to 3 when an iterative method is used for solving the system of equations with multiple right-hand sides, and a speedup factor of 10 when solving this system by a direct method. Using smaller increments increases these speedup factors, and using larger ones decreases them.

## APPENDIX A: THE PADÉ APPROXIMANTS [18]

Suppose that a given function $f(z)$ can be expanded in power series as

$$f(z) = \sum_{i=0}^{\infty} c_i z^i. \tag{23}$$

A Padé approximant of $f(z)$, denoted by $[L, M]$, is

$$[L, M] = \frac{a_0 + a_1 z + \cdots + a_{L-1} z^{L-1} + a_L z^L}{b_0 + b_1 z + \cdots + b_{M-1} z^{M-1} + b_M z^M}, \tag{24}$$

where

$$b_0 = 1. \tag{25}$$

The remainder $b_i$ coefficients are the solution of the following linear algebraic system of equations

$$\begin{bmatrix} c_{L-M+1} & c_{L-M+2} & c_{L-M+3} & \dots & c_L \\ c_{L-M+2} & c_{L-M+3} & c_{L-M+4} & \dots & c_{L+1} \\ c_{L-M+3} & c_{L-M+4} & c_{L-M+5} & \dots & c_{L+2} \\ \cdot & \cdot & \cdot & & \cdot \\ \cdot & \cdot & \cdot & & \cdot \\ \cdot & \cdot & \cdot & & \cdot \\ c_L & c_{L+1} & c_{L+2} & \dots & c_{L+M-1} \end{bmatrix} \begin{bmatrix} b_M \\ b_{M-1} \\ b_{M-2} \\ \cdot \\ \cdot \\ \cdot \\ b_1 \end{bmatrix} = - \begin{bmatrix} c_{L+1} \\ c_{L+2} \\ c_{L+3} \\ \cdot \\ \cdot \\ \cdot \\ c_{L+M} \end{bmatrix}, \tag{26}$$

and the $a_i$ coefficients are given by

$$\begin{aligned} a_0 &= c_0 \\ a_1 &= c_1 + b_1 c_0 \\ a_2 &= c_2 + b_1 c_1 + b_2 c_0 \\ &\cdot \\ &\cdot \\ &\cdot \\ a_2 &= c_2 + \sum_{i=0}^{min(L,M)} b_i c_{L-i}. \end{aligned} \tag{27}$$

Hence, computing the Padé approximant $[L, M]$ requires the knowledge of the first $L + M + 1$ coefficients of the power series (24). This approximant agrees with the truncation of the power series (24) to order $L + M + 1$.

## APPENDIX B: WYNN'S ALGORITHM [19, 20]

The approximation by Wynn's algorithm of the function $f$ defined by its power series (24) consists of constructing a recursive sequence with double entries $(\mathcal{E}_p^n)$ as

$$\begin{aligned} \mathcal{E}_{-1}^n &= 0; && n = 0, 1, 2 \dots \\ \mathcal{E}_0^n &= S_n; && n = 0, 1, 2 \dots \\ \mathcal{E}_{p+1}^n &= \mathcal{E}_{p-1}^{n+1} + \frac{1}{\mathcal{E}_p^{n+1} - \mathcal{E}_p^n}; && n, p = 0, 1, 2 \dots, \end{aligned} \tag{28}$$

where $S_n$ denotes the partial sum of order $n$, that is,

$$S_n = \sum_{i=0}^{n} c_i z^i. \tag{29}$$

Hence, the Wynn algorithm is a recursive procedure that avoids the inversion of any linear system. Similar to the case of the Padé approximants, the construction of $\mathcal{E}_p^n$ requires the knowledge of the first $n + p + 1$ coefficients of the power series (24). When $f$ is a vector valued function ($c_i \in \mathbb{C}^N$), the vector version of this procedure consists of replacing in (28)

the term $\frac{1}{\mathcal{E}_p^{n+1}-\mathcal{E}_p^n}$ by $(\mathcal{E}_p^{n+1}-\mathcal{E}_p^n)^{-1}$, where $y^{-1}$ denotes the inverse of the vector $y$ in $\mathbb{C}^N$

$$y^{-1}=\frac{\overline{y}}{\sum_{i=0}^{N} y_i\overline{y_i}}, \tag{30}$$

and the bar notation is used here to denote a complex conjugate.

## ACKNOWLEDGMENT

The authors acknowledge the support by the Office of Naval Research under Grant N-00014-95-1-0663.

## REFERENCES

1. D. Colton and R. Kress, Inverse acoustic in electromagnetic scattering theory, *Appl. Math. Sci.* **93** (1992).
2. R. P. Shaw, Integral equation methods in acoustics, in *Boundary Elements X*, edited by C. A. Brebia, Springer-Verlag (Berlin/New York, 1988), Vol. 4, pp. 221–244.
3. I. Harari and T. J. R. Hughes, Galerkin/least-squares finite element methods for the reduced wave equation with non-reflecting boundary conditions in unbounded domains, *Comput. Meth. Appl. Mech. Eng.* **98**, 411 (1992).
4. P. Bettes, Infinite elements, *Int. J. Numer. Meth. Eng.* **11**, 53 (1977).
5. D. S. Burnett and R. L. Holford, Prolate and oblate spheroidal acoustic infinite elements, *Comput. Meth. Appl. Mech. Eng.* **158**, 117 (1998).
6. F. X. Roux, Parallel implementation of a domain decomposition method for nonlinear elasticity, in *Domain-Based Parallelism and Problem Decomposition Methods in Computational Science and Engineering*, edited by D. Keyes, Y. Saad, and D. G. Truhlar (Soc. for Inaustr. & Appl. Math., 1995), pp. 161–175.
7. C. Farhat, K. Pierson, and M. Lesoinne, The second generation of FETI methods and their application to the parallel solution of large-scale linear and geometrically nonlinear structural analysis problems," *Comput. Meth. Appl. Mech. Eng.* **184**, 333 (2000).
8. Y. Saad, Iterative methods for sparse linear systems (PWS–Kent, Boston, 1995).
9. M. Malhotra, R. Freund, and P. M. Pinsky, Iterative solution of multiple radiation and scattering problems in structural acoustics using a block quasi-minimal residual algorithm, *Comput. Meth. Appl. Mech. Eng.* **146**, 173 (1997).
10. C. Farhat, A. Macedo, and M. Lesoinne, A two-level domain decomposition method for the iterative solution of high frequency exterior Helmholtz problems, *Numerische Mathematik* **185**, 283 (2000).
11. R. Tezaur, A. Macedo, and C. Farhat, Iterative solution of large-scale acoustic scattering problems with multiple right hand-sides by a domain decomposition method with lagrange multipliers, *Int. J. Nume. Methods Eng.*, in press.
12. B. Engquist and A. Majda, Absorbing boundary conditions for the numerical simulation of waves, *Math. Comput.* **31**, 629 (1977).
13. A. Bayliss, M. Gunburger, and E. Turkel, Boundary conditions for the numerical solution of elliptic equations in exterior regions, *SIAM J. Appl. Math.* **42**, 430 (1982).
14. J. J. Shirron and I. Babuska, A comparison of approximate boundary conditions and infinite element methods for exterior Helmholtz problems, *Comput. Meth. Appl. Mech. Eng.* **164**, 121 (1998).
15. J. M. Jin, *The Finite Element Method in Electromagnetics* (Wiley, New York, 1993).
16. D. S. Jones, Surface radiation conditions, *IMA J. Appl. Math.* **41**, 21 (1980).
17. R. A. Adams, *Sobolev Spaces* (Academic Press, New York, 1975).
18. G. A. Baker and P. Graves-Morris, *Padé Approximants*, 2nd ed. (Cambridge University Press, New York, 1996).
19. P. Wynn, On a device for computing the $e_m(S_n)$ transformation, *MTAC* **10**, 91 (1956).

20. C. Brezinski, *Accélération de la convergence en analyse numérique*, Lecture Notes in Mathematics (Springer-Verlag, Berlin 1977), Vol. 584.
21. X. Antoine, H. Barucq, and A. Bendali, Bayliss–Turkel like radiation conditions on surfaces of arbitrary shape, *J. Math. Anal. Appl*. **229**, 184 (1999).
22. A. G. Ramm, Scattering by obstacles, in *Mathematics and its Applications* (Reidel, Dordreccht, 1986).
23. R. Djellouli, C. Farhat, A. Macedo, and R. Tezaur, Finite element solution of two-dimensional acoustic scattering problems using arbitrarily shaped convex artificial boundaries, *J. Comput. Acoust.* **8**, 81 (2000).
24. C. Farhat, Redesigning the skyline solver for parallel/vector supercomputers, Internat. *J. High Speed Comput*. **2**, 223 (1990).
25. W. Chan and A. George, A linear time implementation of the reverse Cuthill McKee algorithm, *BIT* **20**, 8 (1980).
26. J. P. Berenger, A perfectly matched layer for the absorption of electromagnetic waves, *J. Comput. Phys*. **114**, 185 (1994).
27. J. B. Keller and D. Givoli, Exact non-reflecting boundary conditions, *J. Comput. Phys*. **82**, 172 (1989).